Analyzing the Concurrence of Meteorological Droughts and Warm Periods, with Implications for the Determination of Evaporative Regime

R. D. KOSTER, S. D. SCHUBERT, AND M. J. SUAREZ

Global Modeling and Assimilation Office, NASA Goddard Space Flight Center, Greenbelt, Maryland

(Manuscript received 9 July 2008, in final form 10 November 2008)

ABSTRACT

The hydroclimatic conditions under which a seasonal meteorological drought (below-normal seasonal rainfall) can induce an increase in seasonal air temperature are investigated, first with an atmospheric general circulation model (AGCM) and then with observations. Geographical differences in the dryness–warmth connection abound in the AGCM; in the United States, for example, identified evaporative controls tend to tie meteorological droughts to warmer temperatures in the South but not in the Northeast. The strong agreement between AGCM and observations-based geographical patterns of drought-induced warming supports the idea that the same evaporative controls are also present in nature. A powerful side benefit of the analysis of drought-induced warming is a Northern Hemisphere map, derived solely from observations, showing where total boreal summer evaporation is controlled by soil moisture, energy availability, or both.

1. Background

a. Dry anomalies and temperature anomalies

Linkages between dry and warm conditions are well documented in the literature. Durre et al. (2000) provide an extensive review of the literature and add their own contribution, a detailed joint analysis of soil moisture and daily temperature maxima. They point to Namias (1960) as one of the first studies to identify the likely mechanism for the connection between dry periods and warm periods: drier soil moistures lead to reduced evaporation and thus reduced evaporative cooling. Energy budget constraints suggest that a reduced evaporative cooling is accompanied by an increased sensible heat flux from the surface to the atmosphere (e.g., LeMone et al. 2003), increasing surface air temperature.

Madden and Williams (1978), Chang and Wallace (1987), and Zhao and Khalil (1993) all show that the negative correlation between summertime precipitation and temperature anomalies in the United States is largest in the south-central part of the country and close to zero at both coasts. (To the extent that these studies address the evaporative cooling mechanism, they effectively use precipitation as a surrogate for soil moisture.) Trenberth and Shea (2005) find similar patterns in the observations and extend the analysis to AGCM products. Using model-based soil-moisture estimates, Karl (1986) shows a strong impact of soil moisture on subsequent air temperature in the United States, particularly in the interior of the country, suggesting that soil-moisture estimates can be utilized for forecasting at monthly and longer time scales, a finding echoed by Huang et al. (1996). Shinoda and Yamaguchi (2003) show a clear impact of Sahelian water state on observed air temperature, with lower (absolute) correlations outside of the Sahel.

These studies, which are representative of a broad literature on the subject, all show a geographical variation in the correlation between dry conditions and warm conditions. In the present paper, we use model data and observations to examine these geographical variations in the context of evaporative regime—in particular, the two regimes defined by a well-known nonlinear relationship between evaporation and soil moisture. The two regimes have distinctly different impacts on the potential for drought-induced warming.

b. Evaporative regimes

Climatologists (e.g., Budyko 1974; Eagleson 1978) have long recognized the presence of two distinct hydroclimatic regimes characterizing evaporation from

Corresponding author address: Randall D. Koster, NASA Goddard Space Flight Center, GMAO, Code 610.1, Greenbelt, MD 20771.
E-mail: randal.d.koster@nasa.gov

DOI: 10.1175/2008JCLI2718.1

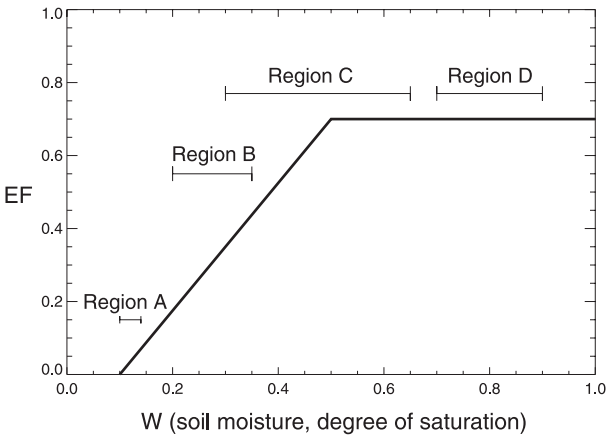

FIG. 1. Idealized β curve relating EF to W. Various soil-moisture ranges are overlain on the plot; see text for details.

the land surface: a drier regime in which increases (decreases) in soil moisture lead to corresponding increases (decreases) in evaporation and a wetter regime in which evaporation is insensitive to soil-moisture changes. To some extent, the two regimes (for simplicity, the soil-moisture-controlled and energy-controlled evaporation regimes) can be explained by vegetation physiology. To conserve moisture, a plant tends to constrict the stomatal apertures on its leaves when the soil surrounding its roots is dry. The reduced apertures impede the flow of water through the plants to the atmosphere, resulting in reduced transpiration and thus reduced total evaporation from the land surface. As the soil wets up, the constriction of the stomatal apertures eases and the plant transpires more. At some level of soil moisture, the plant no longer feels ''water stressed,'' and the apertures are no longer constricted; above this level, further wetting of the soil does not lead to a further opening of the stomata and thus does not lead to additional transpiration. In this latter regime, transpiration, and thus (to a large extent) evaporation, is insensitive to soil-moisture variations. Adding to the distinction in the regimes is the strong nonlinearity in the functional relationship between soil-moisture content and the soil's hydraulic conductivity, a property that describes the ease with which water diffuses toward plant roots or toward the soil surface for bare soil evaporation. The nonlinearity imposes a much greater resistance to total evaporation in the drier regime than in the wetter regime.

Figure 1 illustrates the corresponding highly idealized relationship between evaporative fraction (EF; the ratio of seasonal latent heat flux to total seasonal net radiation) and soil moisture in the root zone (W; expressed as degree of saturation). The two evaporative regimes (again, regimes with a substantial heritage in the literature) are clear in this figure: for drier soil moistures, EF varies with soil moisture and, for wetter soil moistures, it does not—the evaporative fraction is essentially constant. The presence of two evaporative regimes should have a direct impact on how temperature conditions relate to dryness conditions. Because increased evaporative cooling induces reduced surface temperature (and, by extension, reduced near-surface air temperature), seasonal temperature should be sensitive to seasonal soil-moisture variations in the drier regime but not in the wetter regime. It is precisely this distinction that we will seek in the AGCM and in the observational data.

Note that, for convenience, we will often refer in this paper to the response of evaporation to soil moisture though, as indicated in Fig. 1, this is a rather loose interpretation. Over the course of a full season, barring small changes in ground heat storage, the net radiation is partitioned into latent and sensible heat fluxes. Soil moisture, in effect, controls this partitioning; that is, it controls the evaporative fraction rather than evaporation directly. A plot of EF versus soil moisture—at a single point over a number of years or over several points with similar vegetation characteristics—would show much less scatter than a corresponding plot of evaporation versus soil moisture, because evaporation is so strongly tied to the net radiation.

The idealized EF curve in Fig. 1 is, by the way, akin to the β curve employed by land surface models such as the bucket model (Manabe 1969), in which β is defined as the ratio of evaporation to potential evaporation rather than to net radiation. The β curve has the same idealized structure as the EF curve. We use EF rather than β here because an appropriate calculation of the potential evaporation is not straightforward; it requires the difficult determination, given available diagnostics, of equivalent wet temperature (Milly 1992). The basic results of our study would, in any case, be the same.

c. *Framework for analysis*

The presumed operation of such an EF curve in nature, along with the existence of simulated and observed precipitation and air temperature data, provides a unique opportunity to examine evaporative impacts on temperature anomalies. Amano and Salvucci (1999) used temperature signals at the daily time scale at the First International Satellite Land Surface Climatology Project (ISLSCP) Field Project (FIFE) field site to identify transitions between energy-controlled and soil-moisture-controlled evaporation regimes. In the present paper, we focus on seasonally averaged wetness and temperature anomalies over multiple decades with the aim of identifying where, during summer in the Northern Hemisphere, evaporative controls allow anomalously dry conditions at seasonal time scales to induce

anomalously warm conditions at these time scales. [The use of seasonal means rather than daily or weekly values filters out, to some extent, synoptic-scale variability that can affect air temperature independently of land surface moisture state. The use of June–August (JJA) means, rather than, for example, annual means, allows us to focus on a time period for which evaporation should have its strongest impact and helps us to avoid complications regarding interseasonal water storage (Milly 1994).] We first examine multicentury AGCM simulations in detail to isolate unequivocally the relevant operating mechanism behind the dryness–warmth connection within the model. Having solved the problem for the model, we then perform the (necessarily more limited) parallel analysis of purely observational data. We shall see that strong similarities between the modeled and observed signatures of evaporative impacts support the idea that the mechanisms identified for the AGCM are also operating in nature.

Figure 1 shows the four types of regions (A, B, C, and D) we use to illustrate the impact of the EF curve on the dryness–warmth connection. In region D, the range of soil moistures experienced implies that EF never lies in the soil-moisture-controlled regime, meaning that, even in the driest of times, soil-moisture conditions will not lead to reduced evaporation, and thus they will not lead to reduced evaporative cooling and thus warmer temperatures. In region B, however, EF always lies in the soil-moisture-controlled regime, so that drier (wetter) soils generally do lead to warmer (cooler) surface temperatures. Region A also lies in the soil-moisture-controlled regime but its total soil-moisture range is very small so that the impact of soil-moisture variations on evaporation, and thus on surface temperature, is correspondingly small relative to other factors. Region C is particularly interesting because it straddles the two regimes. Wetter periods do not lead to greater cooling, whereas drier periods, in contrast, do lead to greater warming. This nonlinearity marks region C as operating, on average, close to the transition point between evaporative regimes (see further discussion below).

Analogs for these four idealized cases abound in the AGCM and apparently they also exist in nature. In the analyses below, we will examine the relationships between wetness conditions and temperature for these regional types. Because suitable direct observations of soil moisture at the global scale do not exist and because the use of model-based soil moistures, even those based on observed meteorological forcing, would inject unwanted model assumptions into what would otherwise be a purely observational analysis, we characterize JJA wetness conditions for both the model and the observational study with JJA precipitation values rather than with soil moisture itself. We thus neglect for this study the potential impact of antecedent [e.g., March–May (MAM)] precipitation on soil moisture.

2. Model and data

a. AGCM

We use for this analysis the AGCM component of the seasonal forecast system of the Global Modeling and Assimilation Office of the National Aeronautics and Space Administration (NASA). [In earlier studies, this AGCM was referred to as the NASA Seasonal-to-Interannual Prediction Project (NSIPP) AGCM.] All land surface calculations are performed with the Mosaic scheme of Koster and Suarez (1996), a soil–vegetation–atmosphere transfer (SVAT) scheme that uses tiling to account for subgrid vegetation distributions. [See Koster et al. (2000) and Bacmeister et al. (2000) for a more detailed description of the coupled land–atmosphere system and its ability to capture the broad features of the climate system and the global hydrological cycle.]

To ensure reasonable statistics, we examine soil moisture, evaporation, and air temperature data spanning over 600 yr of simulation; the data are extracted from nine parallel 2° × 2.5° simulations covering 1930–2003 and done in the style of the Atmospheric Model Intercomparison Project (AMIP). Again, we examine averages over boreal summer (JJA).

b. Observations used

The precipitation and temperature datasets examined here are the Global Historical Climatology Network (GHCN) global gridded datasets consisting of monthly precipitation and air temperature anomalies at 5° × 5° resolution. (Details about the generation of these datasets are available online at http://www.ncdc.noaa.gov/oa/climate/research/ghcn/ghcngrid.html.) Data in many areas cover the last century. We temporally aggregated the monthly gridded 5° × 5° GHCN data into JJA values. If a month or more of data for a given year was missing, then that year was not included in our analysis.

Of course, no such dataset could ever be free of error. Station density is not homogeneous across time and space; presumably the data provided for some grid cells are based on relatively few stations. Measurement accuracy at individual stations is presumably reduced early in the record. Such limitations must be kept in mind when analyzing the results presented here.

c. Standardization and compositing

When comparing model results with observations, we minimize the impact of AGCM climate bias by performing

the comparisons in terms of standard normal deviates. That is, at a given grid location, the long-term mean (μ) and standard deviation (σ) of quantity X (precipitation or air temperature) are determined and the standard normal deviate X' is computed as

$$X' = (X - \mu_X)/\sigma_X. \quad (1)$$

Different means and standard deviations apply, of course, for the model products and the observations.

Composites of temperature and precipitation (for both unnormalized values and the standard normal deviates) are computed at each grid cell based on precipitation rank. If N is the number of years of JJA precipitation data available, the N yr are separated into 10 deciles of N/10 yr each, with, for example, the lowest decile containing the N/10 driest years and the tenth decile containing the N/10 wettest years. The composited, or decile-averaged, temperature and precipitation for the first decile represent the average JJA conditions for the years with lowest rainfall (i.e., during a meteorological drought).

3. Results: AGCM

a. Diagnosis of underlying EF curve at a grid cell

Analysis of the 600+ yr of AGCM simulation data allows us to identify grid cells that behave like the idealized cases outlined in Fig. 1. This first step involves computing, for context, the full EF–W relationship that would apply at each grid cell if the cell's soil moisture managed to range from completely dry to completely wet (i.e., if the local climatology did not limit the cell's moisture to just a subset of the full range). To compute diagnostically this underlying relationship, we make use of two facts: (i) the relationship between seasonally averaged EF and soil moisture is a strong function of vegetation type and soil texture, and (ii) EF and soil-moisture data from cells with the same dominant vegetation and soil type can be combined into a single plot. Figure 2a shows an example for the case of deciduous broadleaf trees. Each grid cell in the continental United States with this dominant vegetation type (and associated soil texture) provided 600+ yr of seasonal EF–soil-moisture pairs, each of which is shown in the plot. The plot shows some scatter, as might be expected from grid cell variations in secondary vegetation cover and from interannual variations in atmospheric stability and other climatic variables, but the overall shape of the relationship is well defined and the binned curve fitting the points has the expected shape, with the two evaporative regimes clearly displayed: a drier regime in which evaporation is sensitive to soil-moisture variations and a wetter regime in which evaporation is insensitive to soil-moisture variations.

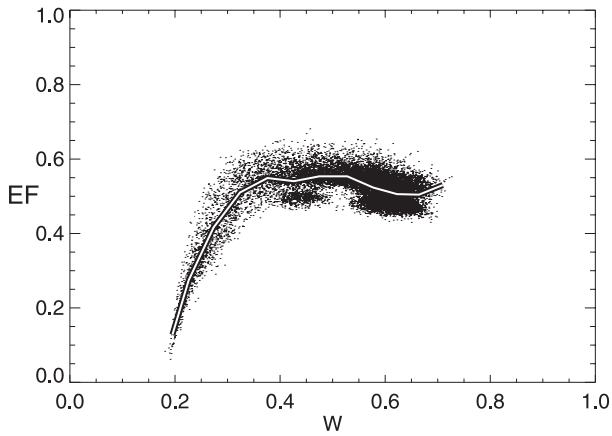

FIG. 2. Relationship between EF for JJA and mean JJA soil moisture (degree of saturation) for U.S. grid cells having broadleaf deciduous trees as the dominant vegetation type. The fitted line was constructed using a simple binning procedure.

Dirmeyer et al. (2006) plotted this functional relationship for a variety of AGCM-based land surface models (see their Fig. 4). For most of the models, they found a similar (if sometimes noisier, probably because of the higher time resolution of the data) kind of relationship. Dirmeyer et al. (2006) also found a clear indication of the relationship from observational data collected in Oklahoma and southern Kansas (see their Fig. 8). In other words, the AGCM used in this paper is not unrepresentative of other models and is not at odds with the limited data available from observations.

b. Examples of temperature–precipitation relationships

Data for the grid cell analogs to the four cases illustrated in Fig. 1 are presented in Fig. 3. (The precise locations of the four cells are indicated in Fig. 4a.) The left-hand panels show the diagnosed EF curves relevant to each grid cell, computed via binning as in Fig. 2. The right-hand panels show the relationships between the composited JJA temperature and precipitation values at the grid cell; the curves for the AGCM are shown with open circles connected by solid lines.

Figure 3a shows results for a grid cell in the northeastern United States. The diagnosed underlying EF curve is, in fact, that computed for Fig. 2. The soil-moisture range for this particular cell is indicated just above the EF curve (the mean soil moisture plus or minus two standard deviations is shown). At this grid cell, evaporation is rarely in the soil-moisture-controlled regime; it thus corresponds to region D in Fig. 1. For reasons outlined above, we expect that, at this point, a

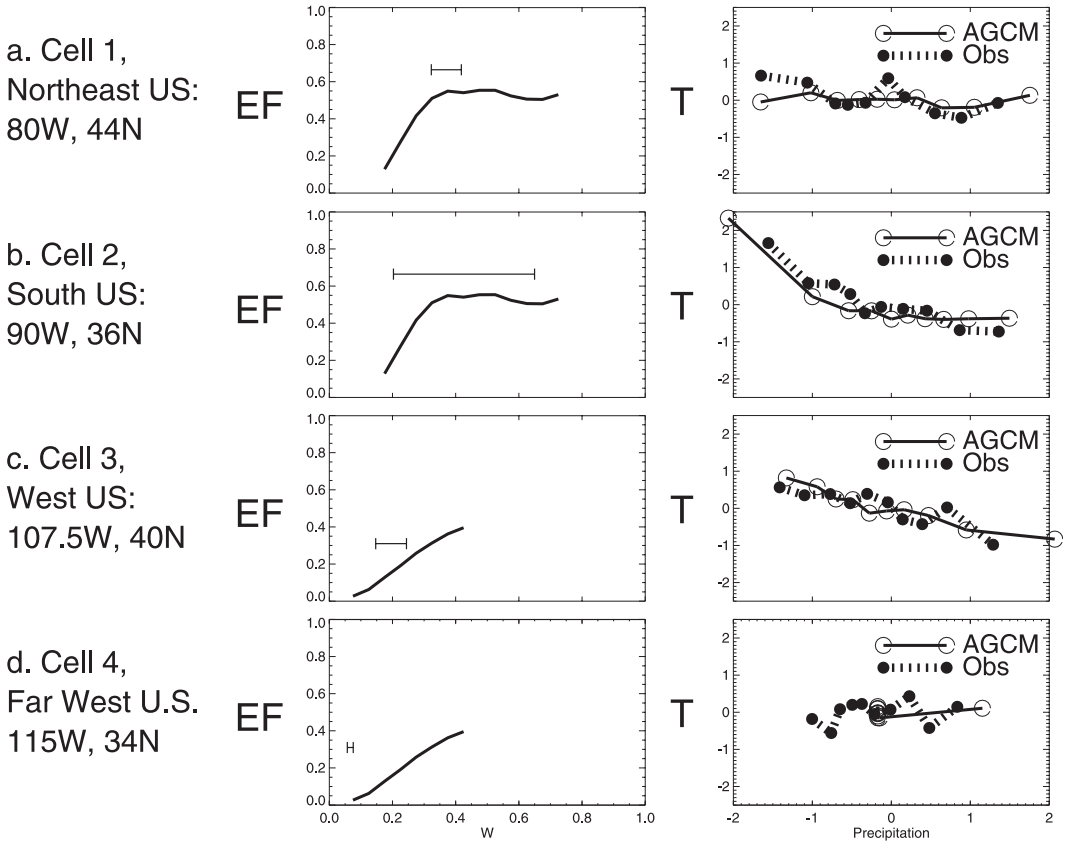

FIG. 3. (left) Average variation of EF as a function of soil moisture for the dominant vegetation type in the AGCM grid cell considered, as diagnosed from a multicentury simulation, using all U.S. grid cells with that dominant vegetation type. The bar above the curve shows the approximate range of root zone soil moisture (mean ± two standard deviations) simulated by the AGCM at the grid cell. (right) Average JJA temperature as a function of composited JJA precipitation for both the AGCM and observations. Temperature and precipitation values are expressed here in terms of standard normal deviates.

given year's JJA temperature will not depend strongly on the wetness conditions (as represented by JJA precipitation) for the year, an expectation borne out by the plotted curve in the right panel of Fig. 3a: the curve relating temperature to precipitation for the AGCM is essentially flat. On average, the grid cell does not get warmer during drier periods.

Figure 3b shows the corresponding plots for a southern United States grid cell. Here, the soil moisture has a large range and evaporation during the driest periods extends into the soil-moisture-controlled regime. For most of the years, however, the evaporation is in the energy-controlled regime. The grid cell is an analog to the idealized region C in Fig. 1, and the temperature–precipitation relationship in the right panel of Fig. 3b meets the aforementioned expectations for such a region: JJA temperature at the cell is not sensitive to wetness (again, as represented by JJA precipitation) during wet periods but is highly sensitive during the driest periods, with the cell becoming significantly warmer during times of drought.

Figure 3c shows the plots for a grid cell in the western United States. Here, evaporation is always in the soil-moisture-controlled regime (corresponding to the idealized region B in Fig. 1), suggesting that the JJA temperature here should always be sensitive to JJA precipitation (the driest years should be warmest and the wettest years should be coolest). This is once again borne out in the right panel of Fig. 3c.

Finally, Fig. 3d shows results for a grid cell in the far west, where the soil-moisture range is very small, making this cell an analog to region A in Fig. 1. The small range of soil moisture in the left panel implies a small range of evaporation and thus a minimal impact on temperature, as seen in the right panel.

c. *Global map of drought-induced temperature increase*

As a simple measure of the degree to which a meteorological drought can induce local warming, we show the composited JJA temperature (standard normal deviate)

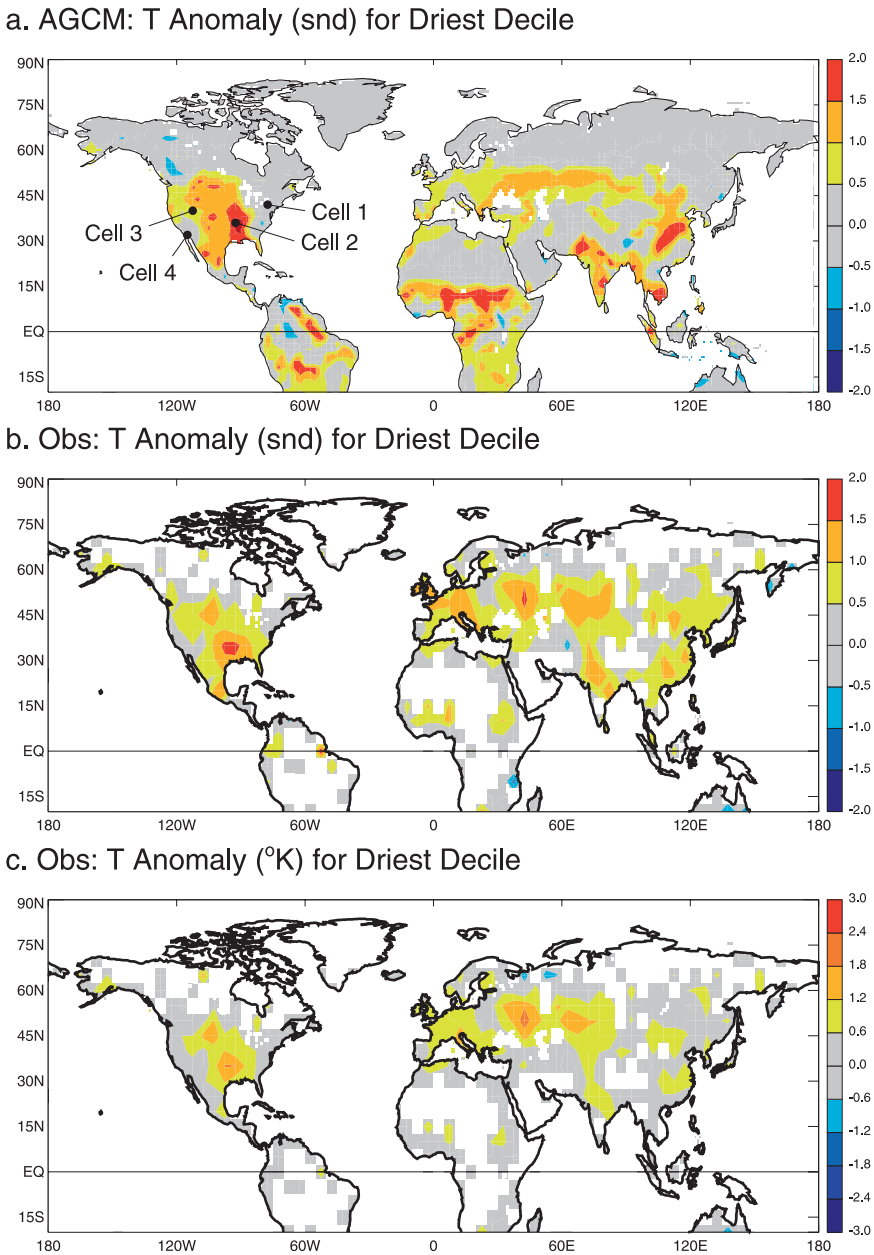

FIG. 4. (a) Composite JJA temperature anomaly (standard normal deviate) for the years with the lowest precipitation (first decile) for the AGCM. (b) As in (a), but for the observations. (c) Averaged temperature anomaly (observations) for the driest precipitation decile, expressed in absolute terms (i.e., in K).

for the lowest precipitation decile in Fig. 4a. Several features are evident in the plot. First, the Mississippi Valley emerges as an area of particularly strong drought-induced warming. This region contains points corresponding to regions B and C in Fig. 1—points for which drought-induced warming is indeed expected. The lack of drought-induced warming in the eastern United States follows directly from the behavior illustrated in Fig. 3a for region D points, and the lack of warming in the far western United States results from the small range of soil-moisture variation there, associated with a small variation in evaporation (Fig. 3d) for region A points.

Across the globe, regions of drought-induced warming are seen along the southern edge of the Amazon, across the Sahel, along a latitudinal band in central

Asia, in India, and in parts of southeastern Asia. These patterns are reminiscent of the ''hotspot'' regions identified in the Global Land–Atmosphere Coupling Experiment (GLACE) project (Koster et al. 2004), regions for which soil-moisture variations were seen to affect rainfall generation across a number of different AGCMs. The agreement is not surprising when one considers that soil-moisture variations would affect both air temperature and precipitation mainly through their effect on the surface energy budget, as represented by the evaporation; this latter effect is maximized, for reasons described above, in regions that are neither too wet nor too dry.

As a further check on our interpretation of the AGCM results, we examined a supplemental AGCM simulation that featured a complete lack of evaporation sensitivity to soil moisture. In this 50-yr AGCM run, we artificially disabled land–atmosphere feedback by prescribing climatological evaporative fractions at each grid cell rather than computing them based on soil moisture. [See Koster et al. (2000) for a complete description of this ''fixed β'' experimental design.] Without evaporation sensitivity to soil moisture, the patterns in Fig. 4a essentially disappear. These results (not shown) demonstrate conclusively that, for the AGCM, the evaporation sensitivity is directly responsible for the patterns seen in Fig. 4a. The patterns are not explained by other potential candidate mechanisms, most notably the reduction of solar radiation (and associated reduced surface temperatures) induced by increased cloudiness (and associated increased precipitation). We thus conclude that these other potential mechanisms are of secondary importance.

4. Results: Observations

Available observations-based soil moisture and evaporation are inadequate for a comparison with model results, so we cannot reproduce the left panels in Fig. 3 for the observations. We can, however, reproduce the right panels; indeed, this was the motivation for plotting temperature against precipitation (rather than soil moisture) in the first place. The right panels of Fig. 3 show how observed JJA temperatures, composited by precipitation amount, vary with observed rainfall (black circles connected by dotted lines) for the $5° \times 5°$ cells containing the plotted AGCM cells. Again, the use of standard normal deviates for both the AGCM and observational results in this figure allow for a comparison of the overall behavior of the model and observational results that is less affected by biases in the AGCM climatology. The agreement between the model and observations is very strong: the observations reproduce the lack of sensitivity in the Northeast and far west, the sensitivity in the west, and, most strikingly, the sensitivity that appears only during the driest periods in the south.

Naturally, not every grid cell shows the observations–model agreement shown in Fig. 3, if only because biases in the model sometimes put a grid cell in the wrong evaporative regime. Even so, the agreement appears to be the rule rather than the exception, as indicated by Fig. 4b. Although the AGCM does show larger temperature (standard normal deviate) anomalies in various regions for the driest decile, another reflection of model bias [notably, a known overactive land–precipitation feedback in this model; see Koster et al. (2003)], the locations of drought-induced warming in nature are highly correlated with those seen in the model, with key areas of warming in the central United States, the latitudinal band across the center of Asia, the northern part of India, and the Sahel. Relative to the model, the observations also show Europe to be a key site of drought-induced warming. Areas for which the observations are insufficient (fewer than 50 yr of coincident JJA precipitation and temperature data) are whited out in the plot.

For reference, Fig. 4c shows the observed temperature anomaly for the lowest precipitation decile expressed in terms of absolute temperature rather than standard normal deviate. Values greater than 1.2 K—a large increase considering that this is an average over the entire summer (JJA) season—appear in parts of the United States and Asia.

5. Using drought-induced warming to derive an observations-based map of evaporative regime

The analysis above supports the idea that the mechanisms responsible for the generation (or hindrance) of drought-induced warming in the AGCM—mechanisms associated with the shape of the EF–W relationship in Fig. 1—are also operating in nature. A simple extension of the analysis allows the construction of a unique and powerful map from the multidecadal temperature and precipitation observations, a map showing where seasonal evaporation is controlled by soil moisture, energy availability, or either (depending on year). In the context of Fig. 1, the map separates continental land areas into A-type, B-type, C-type, and D-type areas.

The first step in the regime-mapping exercise is to establish these areas directly from AGCM soil-moisture and EF data. At a given grid cell, seasonal (JJA) soil moistures over the 600+ yr of simulation are ranked and separated into deciles, in analogy to the ranking and separation of precipitation into deciles (section 2c). The EF values are standardized using Eq. (1) and then averaged over each decile; in particular, we compute the

averages over the driest and wettest deciles, EF_{dry} and EF_{wet}, respectively. Note that when EF_{dry} is nonzero, we can conclude that, at least on the dry end, evaporation is sensitive to soil moisture. Furthermore, a look at Fig. 1 suggests that because EF_{dry} and EF_{wet} are both standardized anomalies, one positive and one negative, their sum should be about zero if evaporation is sensitive to soil moisture throughout the soil-moisture range (a region B point) and nonzero if the soil-moisture range straddles the two evaporative regimes (a region C point), reflecting a curvature in the local evaporation–soil-moisture relationship.

Using this information, with the computed standard deviation σ_w of JJA soil moisture at the cell, we determine whether the grid cell in question is, in the context of Fig. 1, a region A, B, C, or D point as follows (note that the particular values of the coefficients used here are, by necessity, somewhat subjective; nevertheless, reasonable variations in the values lead to qualitatively equivalent results):

(i) Region A: Interannual soil-moisture variations are small enough to prevent interannual evaporation variations from affecting interannual temperature variations. Criterion:

$$\sigma_w < 0.01.$$

(ii) Region B: JJA-averaged evaporation usually lies in the soil-moisture-controlled regime, rarely (if ever) lying in the energy-controlled regime. Criteria:

$\sigma_w > 0.01$ (soil-moisture variations are sufficiently large),
$|EF_{dry}| > 0.3$ (evaporation varies with soil moisture),
$|EF_{dry} + EF_{wet}| < 0.3$ (curvature is small).

(iii) Region C: JJA-averaged evaporation lies in the soil-moisture-controlled regime during some years and in the energy-controlled regime during others. Criteria:

$\sigma_w > 0.01$ (soil-moisture variations are sufficiently large),
$|EF_{dry}| > 0.3$ (evaporation varies with soil moisture),
$|EF_{dry} + EF_{wet}| > 0.3$ (curvature is large).

(iv) Region D: JJA-averaged evaporation usually lies in the energy-controlled regime, rarely (if ever) lying in the soil-moisture-controlled regime. Criteria:

$\sigma_w > 0.01$ (soil-moisture variations are sufficiently large),
$|EF_{dry}| < 0.3$ (evaporation does not vary with soil moisture).

The map in the top panel of Fig. 5 was constructed with these rules. [The rules, by the way, could have been written without the absolute value signs (e.g., $EF_{dry} < -0.3$) with no change in the results; absolute values are used here simply to ease the comparison of the rules with those presented below for temperature and precipitation.] In the map, the colors red, orange, yellow, and blue correspond to region types A, B, C, and D, respectively. The inset in the Pacific illustrates, with the idealized EF curve, what each region type, and thus each color, represents. In effect, this map shows, for the AGCM, the global distribution of evaporative regime operating on the JJA time scale, as determined directly from AGCM-generated evaporation, net radiation, and soil-moisture quantities. It thus shows the geographical distribution of the extent to which variations in soil moisture can affect variations in the surface energy balance and thus—possibly—variations in atmospheric variables, such as rainfall. In the blue and red regions, interannual soil-moisture variations can have no impact on atmospheric variability, whereas in the orange and yellow regions, they can, though with different signatures.

The second step in the regime-mapping exercise is to recognize (as discussed above) that precipitation can serve as a surrogate to soil moisture and (seasonal) air temperature can serve as a surrogate to (seasonal) evaporation, so that an analogous processing of the 600+ yr of AGCM JJA precipitation and temperature values should lead to a map similar to that in the top panel of Fig. 5. Let T_{dry} and T_{wet} represent the (standardized) temperature anomalies for the driest and wettest deciles, as determined from the ranking of JJA precipitation; that is, T_{dry} and T_{wet} are the leftmost and rightmost temperature anomalies plotted in each panel of the right column of Fig. 3. We apply the following rules, which also use the mean JJA precipitation P_{mean} and apply, in effect, the same coefficients as before:

(i) Region A: Interannual soil-moisture variations are small enough to prevent interannual evaporation variations from affecting interannual temperature variations. Criterion:

$|T_{dry}| < 0.3$ (temperature does not vary with precipitation),
$P_{mean} < 1$ mm day^{-1} (rainfall on the low side).

(ii) Region B: JJA-averaged evaporation usually lies in the soil-moisture-controlled regime, rarely (if ever) lying in the energy-controlled regime. Criteria:

$|T_{dry}| > 0.3$ (temperature varies with precipitation),
$|T_{dry} + T_{wet}| < 0.3$ (curvature is small).

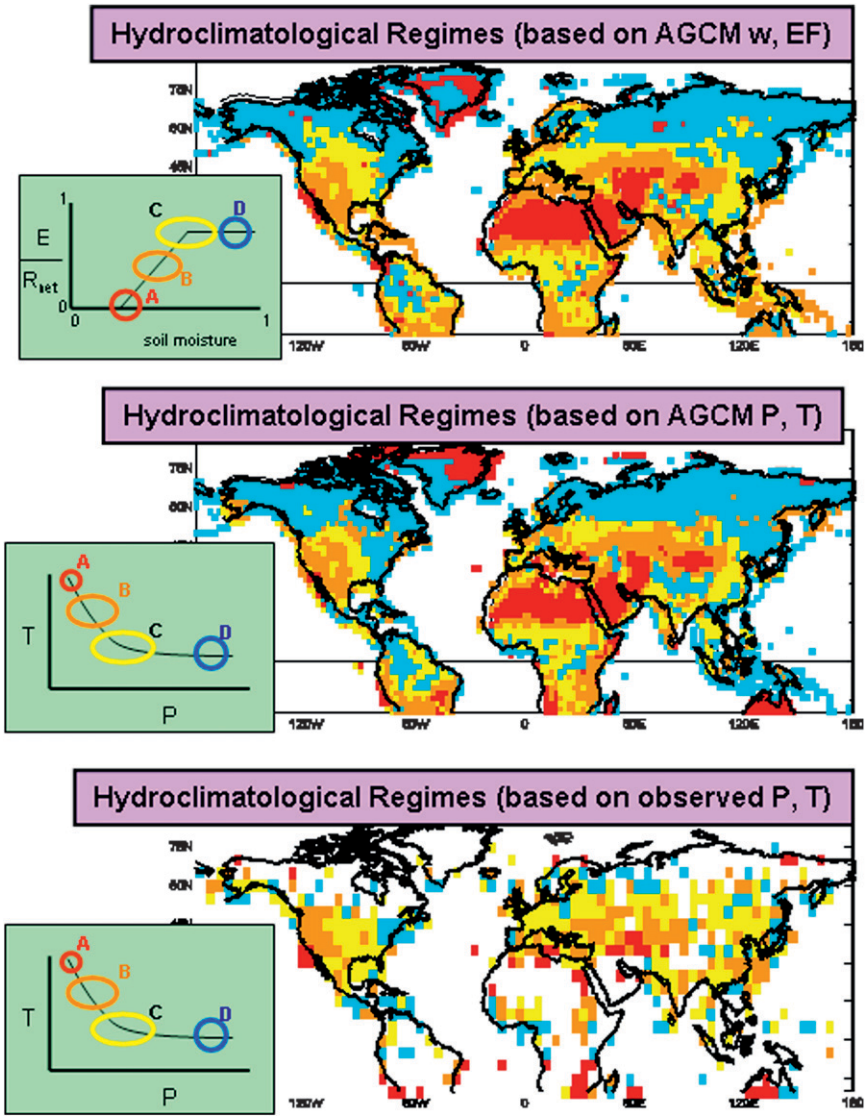

FIG. 5. (top) Identification of hydroclimatological (evaporative) regimes through the rule-based treatment of AGCM-generated JJA evaporation, net radiation, and soil-moisture diagnostics. (See text for details.) (middle) As in (top), but based on AGCM-generated JJA temperature and precipitation diagnostics. (bottom) As in (top), but based on observations-based JJA temperature and precipitation diagnostics. Insets to the maps show the idealized relationships underlying the characterization of the different regimes.

(iii) Region C: JJA-averaged evaporation lies in the soil-moisture-controlled regime during some years and in the energy-controlled regime during others. Criteria:

$|T_{dry}| > 0.3$ (temperature varies with precipitation),
$|T_{dry} + T_{wet}| > 0.3$ (curvature is large).

(iv) Region D: JJA-averaged evaporation usually lies in the energy-controlled regime, rarely (if ever) lying in the soil-moisture-controlled regime. Criteria:

$|T_{dry}| < 0.3$ (temperature does not vary with precipitation),
$P_{mean} > 1$ mm day^{-1} (rainfall on the high side).

The results are plotted in the middle panel of Fig. 5. The inset in the Pacific now illustrates the four region types in the context of an idealized relationship between JJA temperature and precipitation—the one that mirrors that between EF and soil moisture. Note that the $\sigma_w < 0.01$ criterion for region A points is assumed here to be equivalent to the combined $P_{mean} < 1$ mm day^{-1}

and $|T_{dry}| < 0.3$ criteria. We are in effect assuming that, if $|T_{dry}|$ is small despite the region being in the soil-moisture-controlled evaporative regime (as inferred from the low precipitation value), we must have a region A point.

Although the top and middle maps do have their differences, they are generally in very strong agreement. Of course, the agreement is not expected to be perfect, if only because the average JJA soil moisture also depends on rain falling, for example, in April and May. Second-order improvements to the comparison could possibly result from the use of an antecedent precipitation index (API) rather than average JJA rainfall rate. We leave such improvements for future study. The comparison, as it now stands, already supports the idea that a joint analysis of JJA temperature and precipitation can provide much of the same information regarding evaporative regime as a more direct and correct joint analysis of soil moisture and evaporation.

The third and final step in the regime-mapping exercise is to apply the rules elucidated above for JJA precipitation and temperature data to the observational record (i.e., the same data used to produce Fig. 4b). The resulting observations-based map of evaporative regime is shown in the bottom panel of Fig. 5. The observations-based map shows many of the same features as the AGCM-based maps. The transitions from orange to yellow to blue [i.e., from operating strictly in the soil-moisture-controlled regime to operating in both regimes (depending on year) to operating strictly in the energy-controlled regime] are similar when going from west to east in North America and from south to north in central Asia. Important differences, however, do appear. For example, according to the observations, the blue area is greatly reduced in eastern North America and Asia north of Korea. The yellow areas in the observations-based map also extend further to the west in North America.

Such differences may certainly result from deficiencies in the observations; statistics derived from 50 yr of measurements are more subject to error than those derived from 600+ yr of AGCM data, especially given that the observations are often based on a limited number of point-scale (and thus sometimes nonrepresentative) rain gauges, particularly in the early years.

Differences, however, are perhaps more likely to result from biases in the AGCM climate. The presence of climate biases in the AGCM indeed highlights the value of the present analysis. Although the AGCM can serve to demonstrate that temperature and precipitation can be used to isolate evaporative regimes (as indicated by a comparison of the top and middle maps of Fig. 5), it cannot provide a bias-free estimate of where those regimes occur geographically. The observations-based map in the bottom panel of Fig. 5, however, can. This map is of special value because it is, in effect, the best unbiased estimate of evaporative regime distribution possible, because it is not influenced by the assumptions that underlie model formulations. Such a map, of critical importance to a variety of hydroclimatic studies, cannot be produced directly from observations of evaporation and soil moisture, because joint observations of these quantities spanning multiple decades exist almost nowhere.

6. Summary and discussion

Section 1b argues that in the real world, the shape of nature's underlying EF function can explain why the fundamental character of drought may vary geographically; that is, why dry periods tend to induce anomalously warm temperatures in some regions but not in others. Demonstrating this mechanism conclusively with observational data alone, however, is difficult. Although the observed precipitation–temperature relationships in Fig. 3 and the distribution of drought-induced warming in Fig. 4 are consistent with the causal mechanisms suggested by Fig. 1, the causality itself cannot be proven conclusively, because of both the lack of valid observations of soil moisture and evaporation and the overall complexity of the earth's climate system.

This is why the AGCM simulations are useful. With the AGCM data, we demonstrate that the patterns seen in Figs. 4a and 4b result unequivocally from the sensitivity of evaporation to soil-moisture variations, because when we artificially disable this sensitivity, the patterns disappear. Because we know what causes the patterns in the AGCM and the AGCM patterns are so similar to those in the observations (Figs. 3, 4), we infer that—unless the agreement stems from pure chance—the same processes are at work in nature. We can reasonably argue that we understand, for example, the distinction between drought behavior in the U.S. Northeast and south and why only the latter is generally accompanied by warming.

The coincidence of warming with drying has clear implications. Added summer heat implies added societal energy demand and, in some cases, added stress on vegetation growth, in addition to the stress already imposed by lower soil-moisture levels. A more subtle implication of warming involves soil moisture itself. The heating of the ground through reduced evaporative cooling during drought helps reduce soil-moisture levels even further because it increases the saturation vapor pressure at the surface, one of the drivers for evaporation.

In essence, because of this temperature effect, the decline of evaporation rates with decreasing soil moisture is not quite as large as it would be without it and soil moistures can drop slightly further in response to reduced precipitation, perhaps hampering drought recovery.

The analysis of drought-induced warming in sections 3 and 4 lead naturally to a powerful side benefit, a unique and otherwise unobtainable map of evaporative regime based solely on observations (bottom panel of Fig. 5). The map, of course, is not based on direct evaporation and soil-moisture measurements and thus cannot be proven correct. The AGCM, however, convincingly supports the idea that temperature and precipitation data can be used successfully as surrogates for evaporation and soil moisture in the construction of such a map. The bottom panel of Fig. 5 shows where a soil-moisture variation can feed back on evaporation, and thus potentially the atmosphere, in nature. The map should thus prove invaluable to hydroclimatologists interested in land impacts on atmospheric variability. It provides key information on where the measurement of soil moisture is particularly critical for the determination of soil moisture's effects on the atmosphere and thus where, for example, its proper treatment may contribute to the skill of short-term or seasonal weather forecasts.

Acknowledgments. We thank Dara Entekhabi and Chris Milly for useful conversations and two anonymous reviewers for helpful comments.

REFERENCES

Amano, E., and G. D. Salvucci, 1999: Detection and use of three signatures of soil-limited evaporation. *Remote Sens. Environ.,* **67,** 108–122.

Bacmeister, J., P. J. Pegion, S. D. Schubert, and M. J. Suarez, 2000: Atlas of seasonal means simulated by the NSIPP 1 atmospheric GCM. NASA Tech. Memo. 2000-104606, Vol. 17, 194 pp.

Budyko, M. I., 1974: *Climate and Life*. Academic Press, 508 pp.

Chang, F.-C., and J. M. Wallace, 1987: Meteorological conditions during heat waves and droughts in the United States Great Plains. *Mon. Wea. Rev.,* **115,** 1253–1269.

Dirmeyer, P. A., R. D. Koster, and Z. Guo, 2006: Do global models properly represent the feedback between land and atmosphere? *J. Hydrometeor.,* **7,** 1177–1198.

Durre, I., J. M. Wallace, and D. P. Lettenmaier, 2000: Dependence of extreme daily maximum temperatures on antecedent soil moisture in the contiguous United States during summer. *J. Climate,* **13,** 2641–2651.

Eagleson, P. S., 1978: Climate, soil, and vegetation 4. The expected value of annual evapotranspiration. *Water Resour. Res.,* **14,** 731–739.

Huang, J., H. M. Van den Dool, and K. P. Georgakakos, 1996: Analysis of model-calculated soil moisture over the United States (1931–1993) and applications to long-range temperature forecasts. *J. Climate,* **9,** 1350–1362.

Karl, T. R., 1986: The relationship of soil moisture parameterizations to subsequent seasonal and monthly mean temperature in the United States. *Mon. Wea. Rev.,* **114,** 675–686.

Koster, R. D., and M. J. Suarez, 1996: Energy and water balance calculations in the Mosaic LSM. NASA Tech. Memo. 104606, Vol. 9, 60 pp.

——, ——, and M. Heiser, 2000: Variance and predictability of precipitation at seasonal-to-interannual timescales. *J. Hydrometeor.,* **1,** 26–46.

——, ——, Higgins, R. W., and H. M. Van den Dool, 2003: Observational evidence that soil moisture variations affect precipitation. *Geophys. Res. Lett.,* **30,** 1241, doi:10.1029/2002GL016571.

——, and Coauthors, 2004: Regions of strong coupling between soil moisture and precipitation. *Science,* **305,** 1138–1140.

LeMone, M. A., R. L. Grossman, F. Chen, K. Ikeda, and D. Yates, 2003: Choosing the averaging interval for comparison of observed and modeled fluxes along aircraft transects over a heterogeneous surface. *J. Hydrometeor.,* **4,** 179–195.

Madden, R. A., and J. Williams, 1978: The correlation between temperature and precipitation in the United States and Europe. *Mon. Wea. Rev.,* **106,** 142–147.

Manabe, S., 1969: Climate and the ocean circulation. I. The atmospheric circulation and the hydrology of the earth's surface. *Mon. Wea. Rev.,* **97,** 739–774.

Milly, P. C. D., 1992: Potential evaporation and soil moisture in general circulation models. *J. Climate,* **5,** 209–226.

——, 1994: Climate, soil water storage, and the average annual water balance. *Water Resour. Res.,* **30,** 2143–2156.

Namias, J., 1960: Factors in the initiation, perpetuation and termination of drought. International Association of Hydrological Sciences Commission of Surface Waters Publication 51, 81–94. [Available from IAHS Press, Institute of Hydrology, Wallingford, Oxfordshire, OX10 8BB, United Kingdom.]

Shinoda, M., and Y. Yamaguchi, 2003: Influence of soil moisture anomaly on temperature in the Sahel: A comparison between wet and dry decades. *J. Hydrometeor.,* **4,** 437–447.

Trenberth, K. E., and D. J. Shea, 2005: Relationships between precipitation and surface temperature. *Geophys. Res. Lett.,* **32,** L14703, doi:10.1029/2005GL022760.

Zhao, W. N., and M. A. K. Khalil, 1993: The relationship between precipitation and temperature over the contiguous United States. *J. Climate,* **6,** 1232–1236.